Provided for non-commercial research and education use.
Not for reproduction, distribution or commercial use.

Volume 60, 22 October 2012
ISSN 1367-9120
ELSEVIER
Journal of
Asian Earth Sciences
(Formerly the Journal of Southeast Asian Earth Sciences)
Editor-in-Chief
BOR-MING JAHN
See the JOURNAL OF ASIAN EARTH SCIENCES on the World Wide Web
http://www.elsevier.com/locate/jaes

This article appeared in a journal published by Elsevier. The attached copy is furnished to the author for internal non-commercial research and education use, including for instruction at the authors institution and sharing with colleagues.

Other uses, including reproduction and distribution, or selling or licensing copies, or posting to personal, institutional or third party websites are prohibited.

In most cases authors are permitted to post their version of the article (e.g. in Word or Tex form) to their personal website or institutional repository. Authors requiring further information regarding Elsevier's archiving and manuscript policies are encouraged to visit:

http://www.elsevier.com/copyright

Journal of Asian Earth Sciences 60 (2012) 18–30

Contents lists available at SciVerse ScienceDirect

Journal of Asian Earth Sciences

journal homepage: www.elsevier.com/locate/jseaes

Formation of composite dykes by contact remelting and magma mingling: The Shaluta pluton, Transbaikalia (Russia)

B.A. Litvinovsky *, A.N. Zanvilevich, Y. Katzir

Department of Geological and Environmental Sciences, Ben-Gurion University of the Negev, P.O. Box 653, Beer-Sheva 84105, Israel

ARTICLE INFO

Article history:
Received 8 February 2012
Received in revised form 13 July 2012
Accepted 31 July 2012
Available online 10 August 2012

Keywords:
Contact melting
Magma mingling
Composite dykes
Melt inclusions
Transbaikalia
Russia

ABSTRACT

A unique opportunity to study the source areas, from which composite dykes were injected, occurs in the Shaluta pluton, Transbaikalia, Russia. The major quartz syenite pluton was intruded by several synplutonic gabbro bodies of various sizes. Investigations of the contact zones between gabbro and host syenite showed that liquid basalt magma intruded the incompletely crystallized coarse-grained quartz syenite with $T = 700–720$ °C and caused contact remelting of the silicic rock at about 900–950 °C. Mechanical interaction between newly formed silicic melt and partially crystallized mafic magma resulted in extensive magma mingling. Chemical interaction was exhibited by migration of MgO, CaO, FeO*, Sr, H_2O and Cl from the basalt magma, whereas silica, alkalis, Rb and Ba migrated from the silicic refusion zone into the crystallized gabbro. Presence of melt inclusions with homogenization temperature ranging from 640 to 790 °C in quartz and attaining 850–900 °C in late clinopyroxene indicates that at least part of newly formed minerals crystallized from the hybrid melt. Mingled magmatic material was squeezed out inwards, into the host solid quartz syenite pluton and formed dyke-like apophyses that can be traced for a distance of 60–70 m from the contact zone. Apophyses have the same dimensions, structure and composition as typical composite dykes that are common in the roof pendant over the gabbro bodies and nearby the gabbro exposures.

© 2012 Elsevier Ltd. All rights reserved.

1. Introduction

Composite dykes made up of co-mingled silicic and mafic magmas are abundant worldwide. The structure of such composite dykes, their mineral and chemical composition and the petrogenetic aspects of their formation were described in detail (e.g., Wiebe, 1973, 1993; Vogel and Wilband, 1978; Marshall and Sparks, 1984; Furman and Spera, 1985; Kanaris-Sotiriou and Gill, 1985; Zorpi et al., 1991; Wiebe and Ulrich, 1997; Titov et al., 2000; Katzir et al., 2007). Likewise experimental and numerical studies aiming understanding two-phase liquid flow were performed (Kouchi and Sanagawa, 1983; Koyaguchi and Takada, 1994; Snyder and Tait, 1995; Petrelli et al., 2011). Two different types of composite dykes are distinguished: those with silicic margins and those with mafic margins (Snyder et al., 1997; Katzir et al., 2007). Various models of magma mingling in composite dykes have been suggested: (1) intrusion of granitic dykes into an existing chamber of mafic magma permitting the host mafic magma to collapse downward and mingle with still liquid granite dyke (Wiebe and Ulrich, 1997); (2) injection of small batches of mafic magma in partially crystallized silicic melt followed by intrusion of heterogeneous material in the form of composite dykes (Furman and Spera, 1985); (3) intrusion of mingled magmas from completely heterogeneous chamber, irrespective of the mode of its formation (Huppert and Sparks, 1988; Vogel and Wilband, 1978); (4) contact melting followed by mingling of mafic and silicic magmas with subsequent injections of the mingled magmas (Wager et al., 1965; Blake et al., 1965; Litvinovsky et al., 1995); (5) tapping of compositionally stratified magma chamber (Koyaguchi and Takada, 1994). However, none of these models have been supported by convincing field observations. In this paper, field, geochemical, and mineralogical evidence of wholesale remelting of a quartz syenite at the contact with intruded gabbro is presented. The remelting was accompanied by mingling–mixing of silicic and mafic magmas and followed by injection of the magmatic mixture into the granitoid pluton. The injections (large dyke-like apophyses) occur as typical composite dykes with silicic margins. The pressure–temperature conditions and the element behavior during refusion and mingling are estimated.

2. Geological setting

The Shaluta pluton (Fig. 1) is situated in the central part of the Mongolian–Transbaikalian Granite Belt formed during long span of time, from Late Carboniferous through Late Triassic (Wickham et al., 1995; Litvinovsky et al., 1999a, 2011). The pluton is located south of Lake Baikal, in the Selenga River valley, 20 km south of the

---

* Corresponding author. Tel.: +972 8 6461366; fax: +972 08 6477655.
E-mail address: borisl@bgu.ac.il (B.A. Litvinovsky).

1367-9120/$ - see front matter © 2012 Elsevier Ltd. All rights reserved.
http://dx.doi.org/10.1016/j.jseaes.2012.07.018

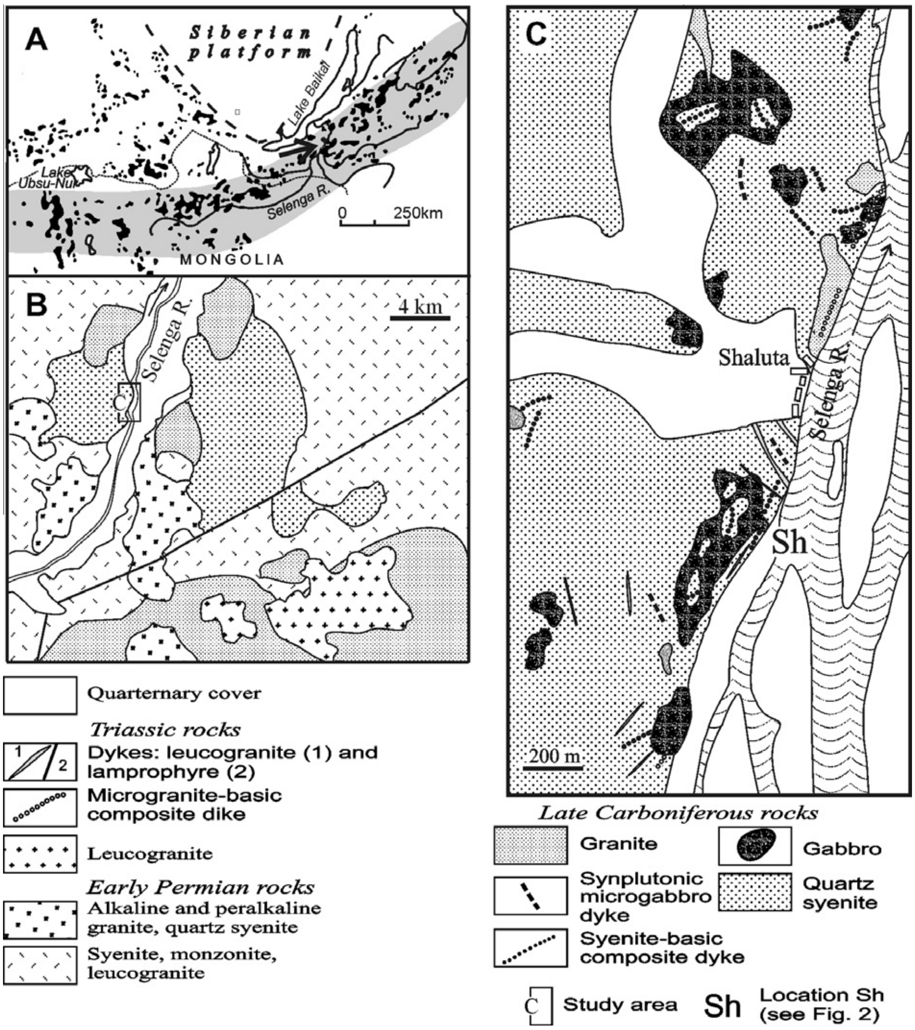
A
Siberian platform
Lake Baikal
Lake Ubsu-Nur
Selenga R.
0 250km
MONGOLIA
B
Selenga R.
4 km
C
Shaluta
Selenga R.
Sh
200 m
Quarternary cover
Triassic rocks
1 2
Dykes: leucogranite (1) and lamprophyre (2)
Microgranite-basic composite dike
Leucogranite
Early Permian rocks
Alkaline and peralkaline granite, quartz syenite
Syenite, monzonite, leucogranite
Late Carboniferous rocks
Granite
Gabbro
Synplutonic microgabbro dyke
Quartz syenite
Syenite-basic composite dyke
C
Study area
Sh
Location Sh (see Fig. 2)

Fig. 1. Geological setting of the Shaluta pluton. (A) Late Carboniferous plutons (black) on the territory of South Siberia and North Mongolia. Shaded area is the Mongolian–Transbaikalian Granite Belt. Location of the Shaluta pluton is marked by an arrow. (B) Geological sketch of the Shaluta pluton. (C) The study area in the central part of Shaluta pluton (see a rectangle in Fig. 1B).

town of Ulan-Ude (Fig. 1A). It occupies an area of about 120 km^2 and constitutes a northern fragment of a much larger, mainly granitic pluton that has been divided into several isolated bodies by Permian syenite–granite intrusions (Fig. 1B). The Shaluta pluton is made up of quartz syenite and smaller irregular bodies of granites; they are referred to as the first and the second intrusive phases, respectively (Fig. 1, B and C). In the central part of the pluton, gabbro bodies of various sizes, from several tens of square meters to 1 km^2, are abundant (Fig. 1C). The similar mineral and chemical composition of gabbro from different bodies, the same interrelations with the host quartz syenite (see below), and positive gravimetric and magnetic anomalies within the area in which the gabbro bodies are exposed suggest that these bodies are projections of an inferred larger basic pluton. The granite of the second phase intrudes both quartz syenite and gabbro. The Shaluta pluton was dated at 288 ± 8 Ma, with $I_{Sr} = 0.7060 \pm 3$, by whole rock Rb–Sr isotope study (Litvinovsky et al., 1999b). Recently U-Pb SHRIMP dating of zircons from two samples of the coarse grained quartz syenite yielded ages of 293 ± 2.5 Ma and 291 ± 1.9 (Y. Katzir, Stanford-USGS SHRIMP Lab.). The detailed description of analytical procedures, samples, and Concordia diagrams will be given in a special paper that is in progress.

Two generations of dykes are distinguished in the area: (1) Earlier, pre-granitic composite dykes consisting of medium-grained quartz syenite with abundant pillow-like and rounded microgabbro enclaves; these dykes are confined to the Shaluta pluton. (2) A Triassic dyke swarm that strikes NE–SW for at least 100 km along the Selenga River valley and intersects both the Shaluta pluton and the Early Permian and Early Triassic plutons to the south of Shaluta (Titov et al., 2000; Litvinovsky et al., 2011). The Triassic dyke swarm comprises mainly aplite, microgranite, composite microgranite–microgabbro dykes and rare lamprophyre. In this paper only the first dyke generation is discussed.

Temporal and spatial relationships between gabbro and coarse-grained quartz syenite of the Shaluta pluton were the main issue of our investigation. Some of the most important details are shown in Figs. 2 and 3 (locations of pictures 3, A and B are shown in the lower right part of Fig. 2). The main feature of the contact zone observed in all outcrops is a decrease in grain size near the contact of both gabbro and quartz syenite. In the gabbro grain size decreases systematically 3–5 times within a zone of 0.3–1 m wide, so that its marginal zone consists of fine-grained, frequently porphyritic microgabbro (Fig. 2, site 2). The contact between the fine-grained rocks in the margin and medium-grained gabbro from the interior is gradational.

The quartz syenites along the border with gabbro become medium-grained, and their transition to the coarse-grained syenite making up the bulk of the pluton is also gradational. Rare irregular

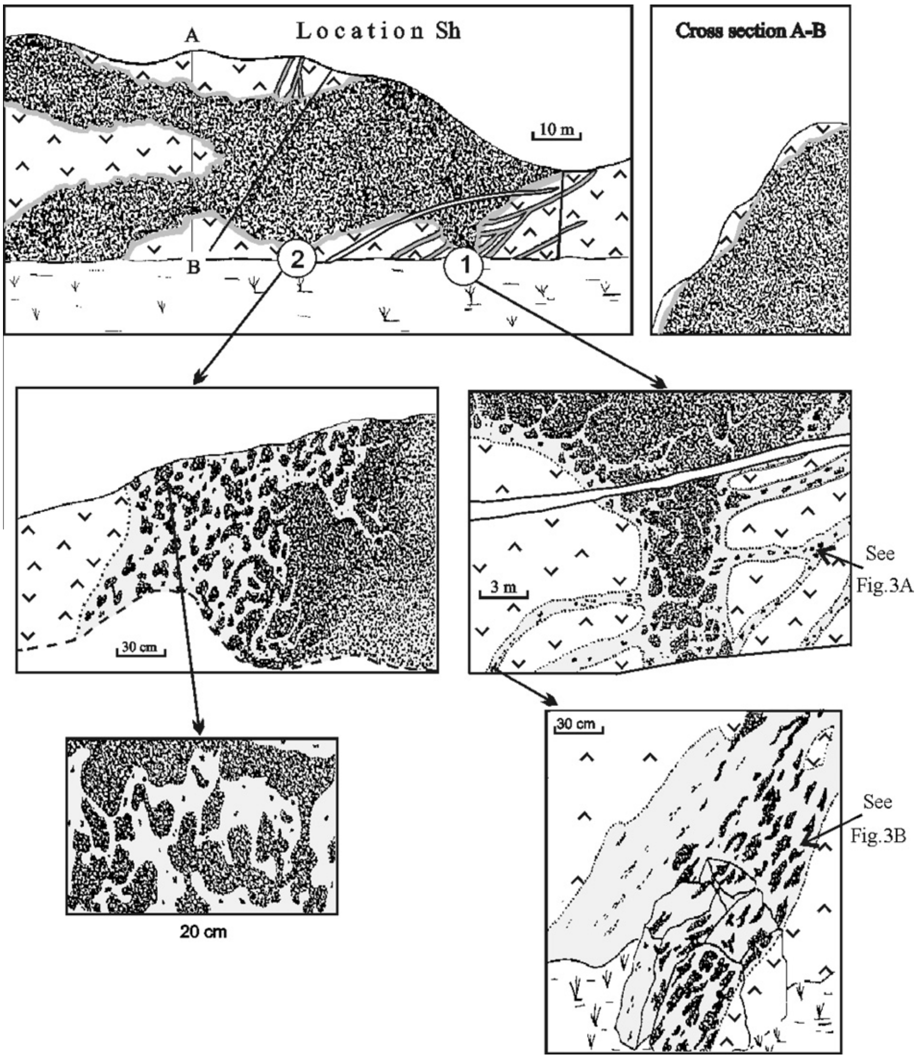

Fig. 2. Field relationships between the intruded gabbro (stippled) and coarse-grained quartz syenite (ticks). Location Sh (see Fig. 1C) is a total view of the outcrop. Dykes in the sketch: dyke-like quartz syenite-microgabbro apophyses (shaded in gray), aplite (white) and the youngest lamprophyre (solid line). The contact zone (off-scale) is also shaded in gray. Structure of the contact zone is shown in detailed sketches of sites 1 and 2. *Site 1*. The contact zone made up of mediun-grained quartz syenite with abundant rounded gabbro enclaves. The dyke-like quartz syenite-microgabbro apophyses are branched off immediately from the contact zone inward the pluton (see a detail in Fig. 3A). In a sketch below is a section of apophysis with evidence of orientation and ductile strain of fine-grained gabbro enclaves (see also Fig. 3B). *Site 2*. The complicated shape of gabbro fragments in the medium-grained quartz syenite (gray) and various stages of their disintegration into rounded enclaves. The darker area is fine-grained and porphyritic gabbro that grades into medium-grained gabbro (stippled area).

and oval patches of medium-grained quartz syenite–granite composition (few tens of centimeters) occur within the host coarse-grained quartz syenite at a distance of several meters away from the gabbro body. As the contact is approached, the patches become more abundant and larger, and immediately near the contact individual patches merge into a continuous zone of medium-grained quartz syenite ranging in width from 0.15 m to 3 m.

Interrelations of the medium-grained quartz syenite with gabbro are fairly complicated. Quartz syenite forms numerous veins that divide gabbro into separate fragments (Fig. 2). Various stages of gabbro disintegration immediately near the contact can be seen in Fig. 2, site 2. As a result of this process, medium-grained quartz syenite frequently contains variable proportions of oval and rounded gabbro enclaves. The enclaves show crenulate, lobate, and scallopped contours oriented convex to the host syenite (Fig. 3, A and C) and evidence of plastic deformation (Fig. 3B and lower right detail in Fig. 2). In some larger enclaves, more than 50 cm in diameter, the core is medium-grained, whereas the peripheral part is made up of fine-grained gabbro. Going deeper into the gabbro bodies, injections of medium-grained syenite are branched out repeatedly, so that eventually a network of thin veinlets penetrates the gabbro to the depth of 5–7 m. Small mafic schlierens and aggregates consisting mainly of plagioclase, amphibole and biotite occur within the medium-grained quartz syenite. Depending on the amount of admixture of mafic material, the composition of silicic rocks in the contact zone ranges from leucocratic quartz syenite to quartz bearing monzonite.

As illustrated in Fig. 2, dyke-like apophyses that are made up of medium-grained quartz syenite with unevenly distributed mafic enclaves branch off the contact zone and are injected into the coarse-grained syenite. The apophyses are up to several tens of meters long, the thickness ranges from 0.3 to 2.5 m. Preferred orientation of enclaves along the strike of some apophyses indicates the direction of magma flow (see the detail of outcrop in the lower right part of Fig. 2 and Fig. 3B).

Some isolated composite dykes made up of medium-grained quartz syenite with abundant mafic enclaves are found within the Shaluta pluton (Fig. 1C). Most of them are located closely to

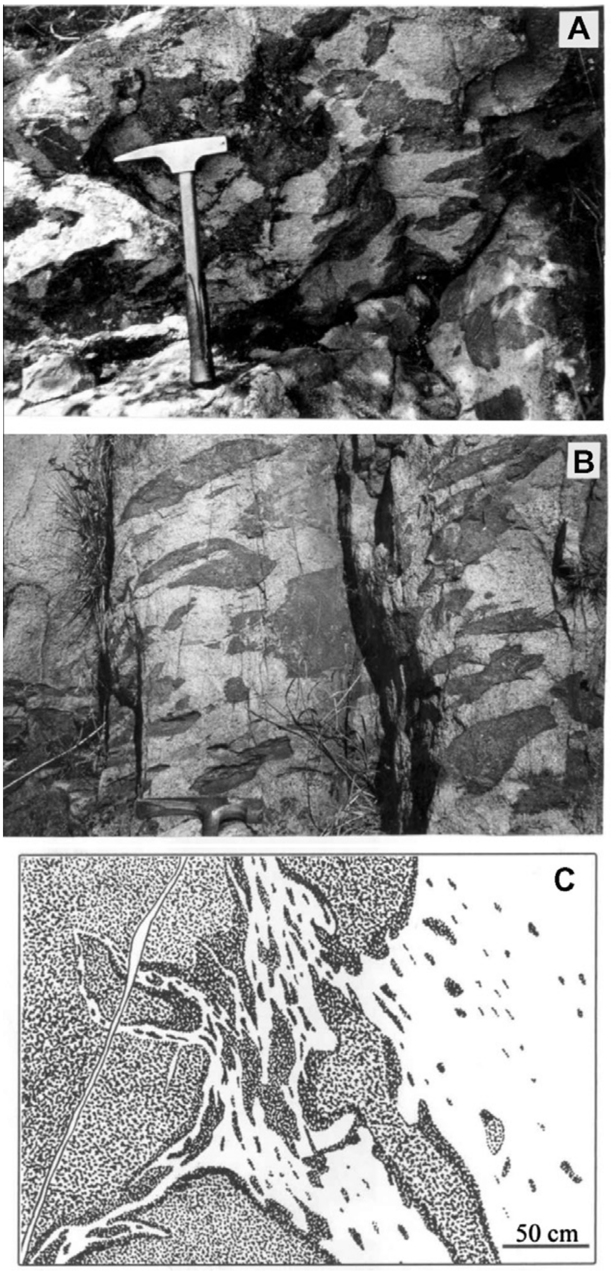

Fig. 3. Outcrop relationships between mafic and felsic rocks in the contact zone. (A) Crenulate and lobate margins of mafic enclaves within the medium-grained quartz syenite (Shaluta outcrop). (*B*) Elongated basic enclaves in the dyke-like apophysis. Enclaves are aligned in conformity with the attitude of the apophysis (Shaluta outcrop). (C) Fragment of the contact that demonstrates complicated curvilinear shape of the medium-grained syenite injection, evidence of ductile deformation of the gabbro fragments and lobate contours of gabbro along the contact (0.6 km to the south, railroad cutting).

the exposed gabbro bodies. The composition and structure of the composite dykes are identical to typical dyke-like apophyses injected in coarse-grained quartz syenite from the contact zone. This suggests that the dykes under consideration are also apophyses formed above the inferred contact zone.

In the vicinity of gabbro bodies, rare microgabbro dykes are found in coarse-grained quartz syenite. Their morphology is typical of synplutonic dykes: dyke-like shape, grain size decrease near the contact and, at the same time, numerous vein-like injections of host quartz syenite. One dyke is especially graphic. It is located at about 100 m NE from the outcrop Sh (Fig. 1C). The microgabbro dyke is exposed in the rocky outcrop for more than 10 m, whereas its width ranges from 5 to 15 cm only. Such a thin dyke is unlikely to produce contact melting in a solid silicic rock. Consequently, numerous injections from the host quartz syenite in the microgabbro indicate that the coarse-grained quarts syenite contained residual melt when the microgabbro dyke was injected.

3. Analytical procedures

3.1. Microprobe analysis

Microprobe analyses were carried out on carbon-coated, polished thin sections using a modernized four-channel MAR-3 electron probe microanalyser at the Geological Institute SB RAS, Ulan-Ude, and Cameca SX-50 at the University of Chicago. Analyses were obtained with a 2–3 μm diameter beam. Operating conditions were 20 kV, beam current of 40 μA, and a counting time of 10 s. Generally 11–13 elements were analyzed, depending on the mineral, and oxygen was calculated by stoichiometry. The detection limits are 0.05–0.09 wt.% for Na_2O, MgO, Al_2O_3, and for SiO_2; 0.01–0.05 wt.% for Cl, K_2O, CaO, TiO_2, MnO, and FeO; 0.3–0.4 wt.% for F.

3.2. Chemical composition

Analysis of the major oxides in all samples and trace elements in selected samples were made by AAS and titration (major elements), XRF (Rb, Sr, Ba, Y, Zr, Nb, and Th), and AES (Co, Cr, Ni and V) at the Geological Institute of RAS, Ulan-Ude. The REE abundance and trace elements in most of the samples were determined at the Analytical Center of Geological Institute of the Russian Academy of Science, Moscow by NAA (REE, Sc, Co, Cr, Hf, and Ta), XRF (Rb, Sr, Ba, Y, Zr, Nb, and Th) and AES (Ni and V). Analytical precision for major elements is ±0.5%, for REE ± 10%, for the rest of the trace elements ±5–10%.

4. Petrography and mineralogy

Quartz syenite making up the bulk of the Shaluta pluton is a pinkish-colored rock with a grain size of 6–8 mm, hypidiomorphic and allotriomorphic texture. It consists of 60–65 vol.% perthitic alkali feldspar (Or_{66-79} Ab_{20-33}) – 12–15% plagioclase (An_{8-14}), 11–15% quartz, and biotite and edenite in roughly equal amounts (3–4 vol.%). Compositions of amphibole and biotite are listed in Tables 1 and 2. In the quartz syenite, occasional zoned plagioclase crystals with up to 48% *An* in corroded cores and rare small aggregates of rounded and isometric plagioclase grains with flakes of biotite are also observed.

Quartz syenite from the contact zone is medium-grained with hypidiomorphic texture, which is exhibited by the predominantly tabular shape of plagioclase and perthitic alkali feldspar with irregular interstitial quartz. The least contaminated leucocratic rocks are homogeneous and similar in mineral composition to the coarse-grained syenite, although plagioclase is 4–6% richer in *An* (Fig. 4.2), whereas amphibole and biotite contain slightly more Ti and less Mn; amphibole is also enriched in Ca (Tables 1 and 2; Fig. 5). Individual larger grains of plagioclase and alkali feldspar that show the same morphology and composition as those of the coarse-grained quartz syenite are abundant (Fig. 4.2). Melting textures, such as strongly corroded edges, clouding and traces of a spongy texture (mainly in plagioclase) are characteristic of some of these grains. Uneven distribution of mafic schlierens and aggregates enriched in biotite and plagioclase causes heterogeneity in the contact zone quartz syenite. These biotite–plagioclase aggregates are indistinguishable from the recrystallized patches in basic

Table 1
Microprobe analyses (wt.%) of amphibole in the representative rock types of the Shaluta pluton.

Sample	zz-2	A248-1	B360	B194-5	B194-9	K4-4		B266	B197-1
No.	1	2	3	4	5	6	7	8	9
SiO_2	45.30	45.62	47.74	48.52	48.37	47.79	46.68	44.11	45.51
TiO_2	0.93	0.96	1.40	1.03	0.94	0.97	1.01	1.31	1.25
Al_2O_3	6.68	7.05	6.32	5.33	5.28	6.86	6.32	8.62	7.50
FeO$*$	17.57	16.43	14.76	16.05	15.24	14.56	15.04	17.33	15.79
MnO	1.64	1.24	0.86	0.83	0.59	0.31	0.25	0.35	0.41
MgO	12.13	13.18	13.02	12.68	14.75	13.34	14.5	11.79	12.79
CaO	11.18	11.35	11.03	11.17	11.51	11.63	11.83	12.36	12.41
Na_2O	1.40	1.63	1.87	1.24	1.27	1.17	1.32	1.13	1.40
K_2O	1.18	1.12	0.80	0.75	0.65	0.66	0.86	0.58	0.86
Cl	0.04	0.07	0.11	0.06	n.d.	0.09	0.10	0.22	n.d.
F	0.77	0.94	0.37	0.34	n.d.	0.01	0.07	0.10	n.d.
	98.82	99.59	98.28	98.00	98.60	97.39	97.98	97.9	97.92
O = F, Cl	0.33	0.41	0.18	0.16		0.02	0.05	0.09	
Total	98.49	99.18	98.1	97.84	98.6	97.37	97.93	97.81	97.92
Atoms to 23 oxygens and 13 cations in (T + C) sites									
Si	6.69	6.657	6.995	7.119	6.946	6.987	6.796	6.545	6.731
Al_{iv}	1.162	1.212	1.005	0.881	0.893	1.013	1.084	1.455	1.269
Fe_{iv}^{3+}	0.149	0.131	0	0	0.161	0	0.12	0	0
Al_{vi}	0	0	0.086	0.04	0	0.168	0	0.051	0.037
Ti	0.103	0.105	0.154	0.114	0.102	0.107	0.111	0.146	0.139
Fe^{3+}	0.943	0.913	0.466	0.608	0.836	0.535	0.759	0.746	0.458
Mg	2.67	2.867	2.844	2.774	3.158	2.907	3.147	2.608	2.82
Fe^{2+}	1.078	0.961	1.343	1.361	0.833	1.246	0.952	1.404	1.495
Mn	0.205	0.153	0.107	0.103	0.072	0.038	0.031	0.044	0.051
Ca_B	1.769	1.775	1.732	1.756	1.771	1.822	1.845	1.965	1.966
Na_B	0.231	0.225	0.268	0.244	0.229	0.178	0.155	0.035	0.034
Na_A	0.17	0.236	0.263	0.109	0.125	0.153	0.218	0.29	0.368
K_A	0.222	0.209	0.15	0.14	0.119	0.123	0.16	0.11	0.162
Sum A	0.392	0.444	0.413	0.249	0.244	0.276	0.378	0.4	0.53

1 and 2 – coarse-grained quartz syenite; 3 and 4 – medium-grained quartz syenite from the contact zone, the least contaminated (3) and contaminated (4); 5 – hybrid quartz-bearing monzonite; 6–9 – medium-grained gabbro, the least hybridized (6 and 7) and hybridized (8 and 9). Here and in Table 2: FeO* = Fe total as FeO; n.d. = not determined.

Table 2
Microprobe analyses of biotite and pyroxene in the representative rock types of the Shaluta pluton.

Sample	zz-2 1	A248-1 2	B360 3	B194-5 4	B194-9 5	K4-4 6	B266 7	B197-1 8	A438 9	B266 10
SiO_2	39.98	39.51	38.51	38.72	37.26	35.43	35.39	36.09	36.7	52.54
TiO_2	1.05	1.16	2.28	2.31	2.78	3.33	3.21	3.20	1.42	0.26
Al_2O_3	11.89	11.82	11.98	11.75	13.12	13	12.72	12.81	12.93	1.48
FeO$*$	14.43	14.64	16.9	17.31	18.5	19.37	21.2	20.28	16.82	9.49
MnO	1.04	0.75	0.66	0.70	0.27	0.15	0.3	0.22	0.49	0.32
MgO	16.19	16.46	14.63	14.04	13.49	14.08	12.8	13.41	17.05	13.28
CaO	–	–	0.03	–	–	–	–	–	0.08	21.29
Na_2O	–	–	0.1	0.11	0.1	–	0.17	0.18	0.20	0.56
K_2O	10.52	10.39	10.42	10.25	10.15	10.25	9.98	10.25	10.57	–
Cl	0.1	0.16	0.23	0.17	n.d.	0.26	0.29	n.d.	n.d.	n.d.
F	2.05	1.93	1.09	0.52	n.d.	0.12	0.22	n.d.	n.d.	n.d.
O = F, Cl	0.89	0.85	0.51	0.26		0.11	0.16			
Total	98.14	97.67	97.37	96.14	95.67	96.1	96.44	96.44	96.26	99.22
	O = 11									O = 6
Si	3.005	2.983	2.923	2.951	2.841	2.732	2.747	2.767	2.778	1.981
Al_{iv}	0.995	1.017	1.072	1.049	1.159	1.181	1.164	1.158	1.154	0.019
Ti_{iv}			0.005			0.087	0.089	0.075	0.068	
Al_{vi}	0.058	0.034		0.006	0.02					0.015
Ti_{vi}	0.06	0.066	0.125	0.133	0.159	0.106	0.099	0.109	0.013	0.005
Fe	0.907	0.924	1.073	1.104	1.18	1.249	1.376	1.3	0.065	0.787
Mn	0.066	0.048	0.042	0.045	0.017	0.009	0.02	0.014	0.031	0.010
Mg	1.814	1.853	1.656	1.595	1.534	1.618	1.481	1.532	1.924	0.787
Ca										0.888
Na			0.015	0.017	0.015		0.026	0.027	0.029	0.032
K	1.009	1.001	1.01	0.997	0.988	1.008	0.988	1.002	1.02	

Biotite: 1 and 2 – coarse-grained quartz syenite; 3 and 4 – medium-grained quartz syenite from the contact zone, the least contaminated (3) and contaminated (4); 5 – hybrid quartz-bearing monzonite; 6–8 – medium-grained gabbro, the least hybridized (6) and hybridized (7 and 8); 9 – fine-grained porphyritic gabbro from the marginal zone of gabbro body. *Clinopyroxene*: 10 – medium-grained gabbro, the later assemblage.
"–" = below the limit of detection.

enclaves. Similar to the enclaves, the mafic schlierens contain rare prismatic crystals of zoned plagioclase with up to 34% *An* in the core and 20% An in the marginal zone (Fig. 4.2). These observationsis indicate variable extent of contamination of silicic magma by

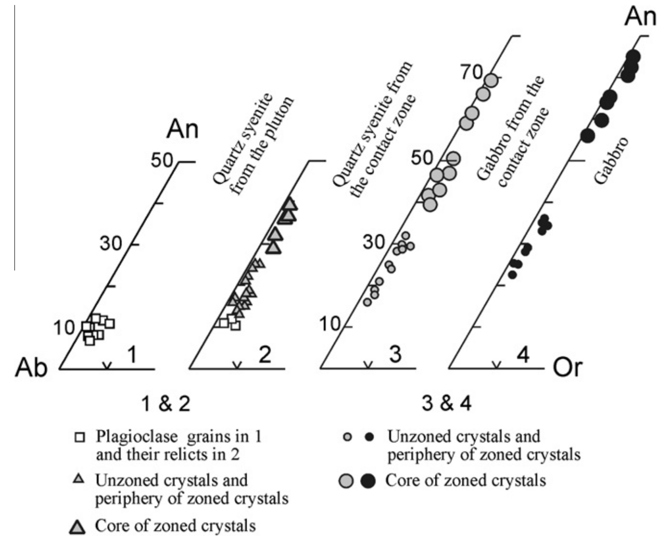

Fig. 4. Composition of plagioclase from magmatic rocks of the Shaluta pluton plotted on the diagram *Ab–An–Or*.

gabbroic material. The contaminated varieties of medium-grained quartz syenite range in composition from quartz syenite to quartz bearing monzonite. The latter is highly heterogeneous, porphyritic, with numerous rounded basic enclaves. Phenocrysts in this rock are prisms of zoned plagioclase with about 40% *An* in the core (Fig. 4.2). In the matrix, plagioclase (20–26% *An*) dominates over alkali feldspar; interstitial quartz constitutes 5–10 vol.% of the rock. The hornblende and biotite compositions are similar to those in gabbro (Tables 1 and 2; Fig. 5).

Gabbroic rocks described here include gabbro from the inner pluton and gabbro from the marginal zones. The most typical gabbro of the inner pluton is a medium-grained rock with a grain size of 2–4 mm. The texture is hypidiomorphic and in places subophitic. The presence of two different mineral assemblages in widely variable proportions is characteristic of these rocks. The early assemblage includes Ca-rich plagioclase (65–75% *An*), hornblende and heavily altered clinopyroxene. The late assemblage consists of andesine (28–38% *An*), edenite, biotite, rare fresh clinopyroxene, minor alkali feldspar and quartz. Ca-rich plagioclase is found only in the corroded cores of zoned crystals (Fig. 4.4), whereas early pyroxene and hornblende are replaced to various extents by edenite and biotite. The late assemblage is especially abundant at the marginal zones of gabbro residing near the contact with quartz syenite; therefore the assemblage is taken as an evidence of hybridization of gabbro.

In gabbro from the marginal zone porphyritic texture and decrease in grain size are common. The amount of phenocrysts (plagioclase only) is about 10% at the immediate contact with syenite. The proportion of minerals of the later assemblage progressively increases, up to 80–90%. Plagioclase is impoverished in *An* both in phenocrysts and in the matrix, though in the core of some phenocrysts a plagioclase with 65–70% *An* is also found (Fig. 4.3).

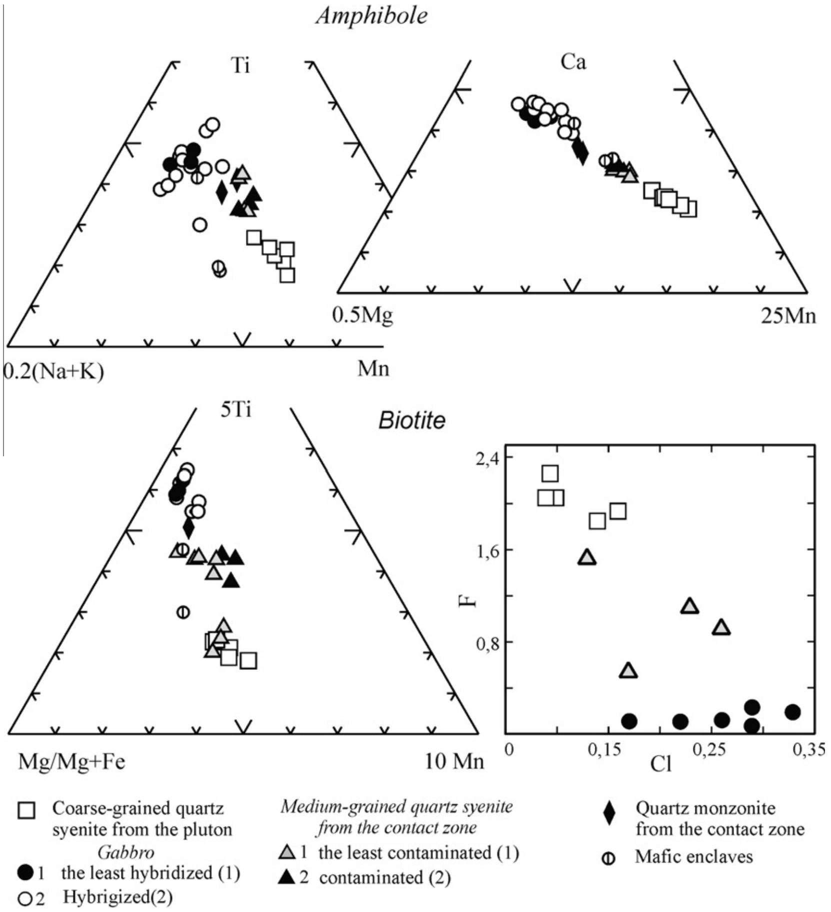

Fig. 5. Composition of amphibole plotted with respect to 0.2(Na + K)–Ti–Mn, 0.5 Mg–Ca–25Mn, and biotite plotted with respect to Mg/(Mg + Fe)–5Ti–10Mn and in F vs. Cl diagram.

5. Chemical composition

Major and trace element whole-rock compositions were determined in 49 samples; of them, 14 samples were analyzed for REE. The results are plotted in Figs. 6–8, and data for a subset of 43 most representative samples are reported in Table 3.

Fig. 6 shows the variations of selected major and trace elements in coarse-grained quartz syenite from the bulk of the Shaluta pluton and in medium-grained varieties from the contact zone. Both coarse-grained and leucocratic (the least contaminated) medium-grained rocks are characterized by narrow range of SiO_2 content (from 64.5% to 67.5%) and no evident correlation between SiO_2 and other major oxides (Fig. 6A). The compositions of these two groups of rocks overlap for almost all major elements (the diagram for MgO vs. SiO_2 is similar to that for FeO*, not shown), as well as for many trace elements, including REE (Fig. 7A). Only Ba and Sr in medium-grained quartz syenite from the contact zone are significantly higher, though correlation between Sr and CaO, Ba and K_2O is not exhibited (Fig. 6B). Contamination by the gabbro material, as a whole, causes decrease of SiO_2 and increase of FeO*, MgO and CaO, as well as Cr, Ni and Co (Fig. 6A; Table 3).

The chemical composition of gabbro is shown in a set of variation diagrams (Fig. 8) and REE patterns (Fig. 7B). Samples shown in the plots were collected from the least hybridized varieties of rocks, in which the late mineral assemblage constitutes less than 10–15%. The silica content in these rocks ranges from

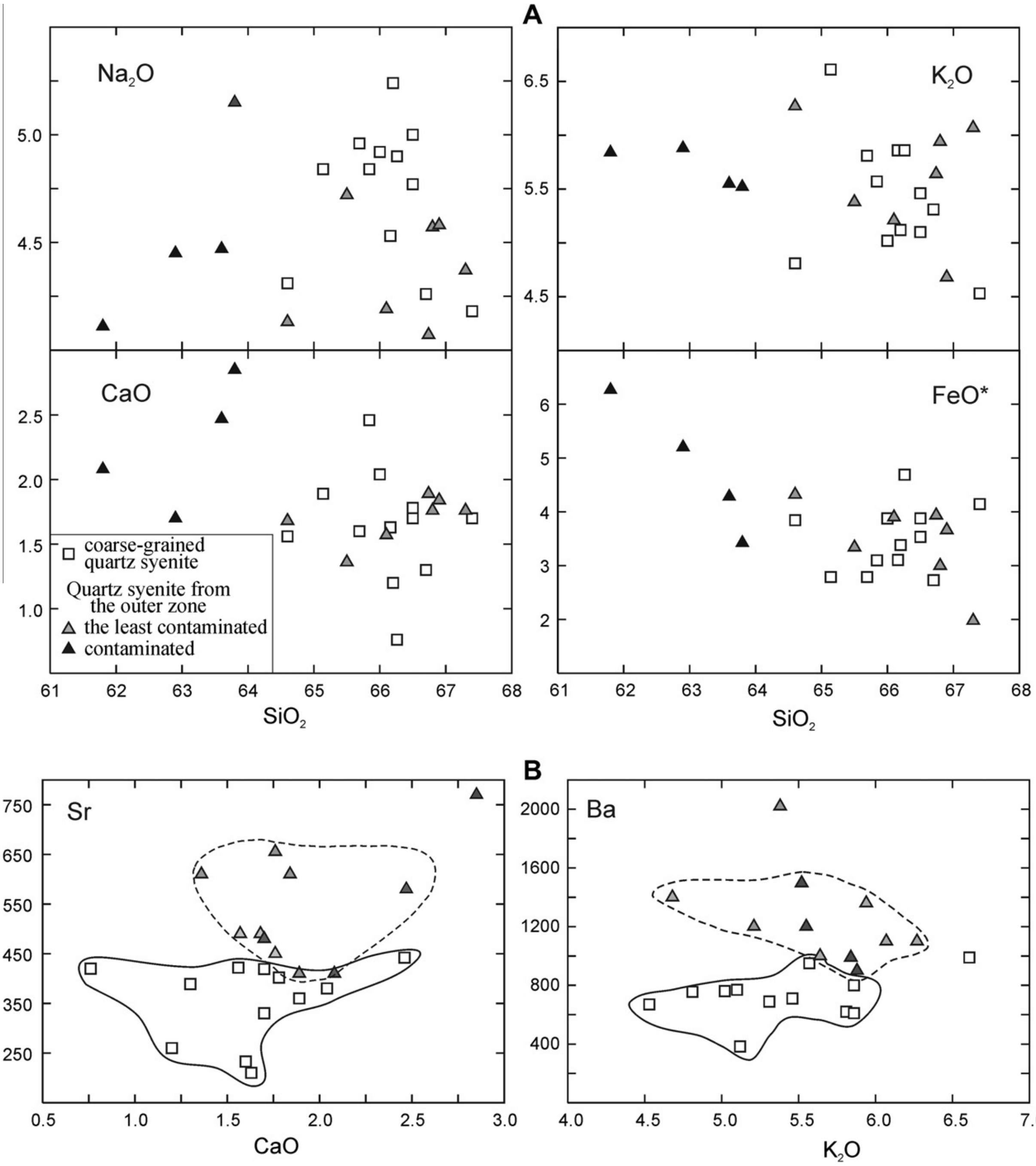

Fig. 6. Variation diagrams for selected major and trace elements for quartz syenite. (A) SiO_2 vs. Na_2O, K_2O, CaO, FeO*. (B) CaO vs. Sr and Ba vs. K_2O. Major oxides as wt.%, trace elements as ppm.

Table 3
Major (wt.%) and trace element (ppm) compositions of igneous rocks from the Shaluta pluton.

Rock	Least hybridized gabbro				Gabbro hybridized to various extent (5–22)																		Medium-grained qtz syenite, contaminated				Medium-grained qtz syenite, leucocratic						Coarse-grained qtz syenite (33–44)											
Sample	B45-5	K4-4	K4-5	B197-9	M60-15	K4-3	B197-8	B197-2	K183-2	B197-7	B266	K43-8a	B196-6	K183-11	B194	A248-4	B152	B196-11	K183-12	M60-2	B197-6	B196-5	A436-10b	A436-10a	B421	B269	A438-1b	A436-9a	A248-2	B196-8	A436-9	B196-7	K45	A248	136a	B45-1	K-4A	B118	K49	M60	A248-1	K45-6	B196-10	K-4B
Number	1	2	3	4	5	6	7	8	9	10	11	12	13	14	15	16	17	18	19	20	21	22	23	24	25	26	27	28	29	30	31	32	33	34	35	36	37	38	39	40	41	42	43	44
SiO_2	50.2	50.5	50.3	51.5	50	50	50.8	51	51.1	51.1	51.3	51.2	51.8	52.6	53.8	53.32	53.5	53.5	53.6	53.04	54.4	55.1	61.8	62.9	63.6	63.8	64.6	66.1	66.74	66.8	66.9	67.3	64.6	65.14	65.69	65.84	66	66.16	66.2	66.26	66.5	66.5	66.7	67.4
TiO_2	0.87	0.86	0.84	0.89	0.98	0.95	1.05	1.13	0.95	1.06	1.09	0.94	1.13	1.08	1.1	0.94	1.04	0.94	1.06	0.96	0.89	0.96	0.87	0.8	0.55	0.6	0.72	0.32	0.44	0.4	0.4	0.39	0.51	0.42	0.43	0.41	0.67	0.48	0.56	0.27	0.34	0.41	0.36	0.63
Al_2O_3	14.1	15.9	14	15	16.65	17	18.5	18	16.8	18.9	17.2	17.65	17.16	17.1	16.7	16.82	17.45	17.5	16.9	18.48	17.7	16.66	16	16	16.9	16.9	15.6	16.35	16.12	16.2	15.9	15.5	16.75	17.28	16.83	15.54	16	16.6	16.3	16.38	16.18	16.4	16.4	15
Fe_2O_3	3.24	2.25	2.94	7.49	3.44	2.39	7.91	2.94	3.61	7.91	8.13	2.48	7.51	4.55	3.06	5.38	3.66	8.57	3.98	3.23	7.1	3.3	3.34	3.58	2.27	3.36	2.3	2.31	2.54	0.91	1.98	0.73	1.77	2.13	1.73	1.92	1.94	1.45	3.27	3.8	1.72	3.37	2.7	2.37
FeO	5.34	6.41	5.79	1.36	5.34	6.05	1.2	5.7	5.46	1.2	1.52	6.14	1.59	4.37	4.54	4.41	4.48	1.22	4.76	4.38	1.1	4.45	3.26	1.98	2.24	0.4	2.25	1.82	1.65	2.18	1.88	1.32	2.25	0.87	1.23	1.37	2.13	1.8	0.44	1.27	2.33	0.5	0.3	2.01
MnO	0.18	0.18	0.18	0.13	0.14	0.15	0.13	0.15	0.13	0.12	0.14	0.17	0.16	0.14	0.17	0.15	0.13	0.16	0.14	0.13	0.13	0.19	0.05	0.06	0.05	0.07	0.04	0.04	0.09	0.09	0.05	0.09	0.11	0.07	0.08	0.03	0.09	0.06	0.07	0.08	0.08	0.07	0.06	0.08
MgO	9.3	7.28	9.4	8.37	6.21	6.08	4.4	4.42	5.87	3.48	5.88	5.12	4.12	4.11	4.46	4.02	4.19	3.78	3.9	4.01	3.98	3.98	1.1	0.71	1.01	0.7	0.8	0.58	0.56	0.63	0.96	0.63	0.71	0.2	0.69	0.8	0.76	0.54	0.4	0.5	0.44	0.54	0.37	0.66
CaO	8.23	9.45	8.25	8.23	7.51	7.51	7.6	7.78	6.51	6.96	6.74	6.15	7.24	6.27	6.59	7.29	5.9	5.88	6.01	5.03	8	4.96	2.08	1.7	2.47	2.85	1.68	1.57	1.89	1.76	1.84	1.76	1.56	1.89	1.6	2.46	2.04	1.63	1.2	0.76	1.78	1.7	1.3	1.7
Na_2O	3.22	3.47	3.62	2.93	4.28	4.34	3.98	4.16	3.7	3.57	3.51	4.18	4.29	4.4	3.96	3.53	3.95	4.6	4.2	4.2	3.35	4.9	4.11	4.45	4.47	5.15	4.13	4.19	4.07	4.57	4.58	4.37	4.31	4.84	4.96	4.84	4.92	4.53	5.24	4.9	5	4.77	4.26	4.18
K_2O	2.62	2.23	2.52	2.2	3.08	3.22	2.35	2.43	3.22	3.12	2.39	2.53	3.24	2.95	3.31	3	3.17	2.2	3.06	3.45	2.16	2.9	5.84	5.88	5.55	5.52	6.27	5.21	5.64	5.94	4.68	6.07	4.81	6.61	5.81	5.57	5.02	5.86	5.12	5.86	5.1	5.46	5.31	4.53
P_2O_5	0.43	0.34	0.38	0.43	0.68	0.53	0.6	0.54	0.27	0.52	0.17	0.44	0.48	0.32	0.51	0.37	0.4	0.43	0.28	0.44	0.35	0.41	0.28	0.26	0.16	0.11	0.22	0.14	0.12	0.15	0.18	0.07	0.16	0.06	0.14	0.14	0.23	0.07	0.1	0.09	0.09	0.14	0.1	0.2
LOI	2.1	1.35	1.85	1.95	1.75	2.05	1.18	2.13	2.6	1.46	1.27	3.41	1.37	2.38	1.7	0.48	1.79	1.64	2.22	1.41	1.42	2.39	0.86	1.11	0.54	0.94	0.85	0.8	0.12	0.54	1.1	0.8	2.02	0.48	0.62	0.87	0.23	0.24	0.8	0	0.71	0.51	1.58	0.83
Total	99.83	100.22	100.1	100.48	100.06	100.3	99.7	100.38	100.22	99.4	99.34	100.41	100.09	100.27	99.9	99.71	99.66	100.42	100.11	98.76	100.58	100.2	99.59	99.43	99.81	100.4	99.46	99.43	99.98	100.17	100.45	99.03	99.56	99.99	99.81	99.79	100.03	99.42	99.7	100.2	100.27	100.37	99.44	99.59
Rb	96	65	100	56	89	90	80	65	120	83	65	133	130	80	82	78	107	140	80	100	67	143	170	190	120	146	215	170	150	146	140	190	166	168	171	155	160	155	159	160	169	159	173	170
Ba	930	893	900	946	1400	1400	1250	1300	1000	1480	995	990	1400	1300	1200	1270	1250	1350	1300	1300	1070	867	990	900	1200	1497	1100	1200	1000	1360	1400	1100	756	990	620	950	760	610	383	800	770	710	689	670
Sr	870	920	930	1100	1100	1200	1300	1300	1150	1300	1200	1049	1400	1100	1000	1046	1004	1400	1100	1300	1182	1061	410	480	580	770	490	490	410	655	610	450	422	360	233	442	380	210	260	420	402	419	389	330
Zr	160	140	160	155	240	310	194	180	150	200	119	110	210	200	198	158	168	210	190	230	119	172	340	310	360	344	240	200	310	362	250	330	398	378	427	215	470	330	509	410	248	386	294	390
Y	19	35	30	25	22	21	27	24	18	28	27	28	26	22	26	21	30	26	18	21	26	30	43	36	35	30	23	22	30	31	20	45	32	35	48	15	40	36	59	33	21	26	23	35
Nb	8.3	12	15	12	10	13	12	9.8	11	10	11	8.9	11	7	14	14	20	10	8	10	12	24	34	34	26	16	22	13	26	19	9	36	42	30	30	21	38	25	35	43	30	34	29	36
Th	5.9	4	0		4.4	0		2.9			11	9.6	8.5		13							11	34		24	19		21	0	20		36	22				3.9		32			16	12	29
Cr	520	250	250		120	89.1		57			97		16		110		34.6					23.1	8					9	14.4	7.5		11		11.5		20	9.6	3.5		9.3				5.4
Ni	85	76	43.6		55	33.1		20			36		34.3		42		25.1					37.3	3					7	9.1	8.5		7		4		6.2	3	5		10				3
Co	34	36	16.6		29	14		26			31		21		25		14					27	2					2	2.8	3.6		2.7		3.4		3	3.1	2.6		3				2.2
Sc		30						0							18																	0		0		0	0	4.7	4.7					
V	85	195	46.7		85	81.2	39	120			100		50		165		128.8					110	16					14	43.7	33.5		45		30.2		23	17	45	0	37.2				10
Cu	27	0	29	35	45	34	39	35		22	61	22	24		28	2.8	14	22			31	15		24		11			8.2	14		13	13	9.8		10	22	4	11	9	12	17	13	26
Zn	71	68	74	100	63	68	130	89		110	120	87	79		81	7.9		120			90	96		24		39			23	47		49	42	19		20	9.6	3.5	73	18	24	42	33	5.4
Li	20	28	26	23	21	21	33	29		26	30	37	33		34	6		51			17	37		25		21			20	27		21	18	15		33.1	24	9	33	7	19	18	25	23
Ta	0.45	0.38			0.54			0.42				0.55	0.62		0.66								1.3					1				2.7					1.9							1.3
Hf	2.6	3.4			3.9			3.2				4.1	5		6.3								6.1		10			5.1				10					7.3							5.3
La	42	43			40			48				46	49		52								41		19			72				88					55	84						52
Ce	87	100			87			100				93	97		100								79		30			110				180					100	180						68
Nd	34	42			36			37				34	35		42								28		11			35				66					31	70						16
Sm	6.3	8.4			6.4			7.3				6	6.4		7.2								4.3		1.1			4.1				9.7					4.7	9.3						2.4
Eu	1.7	1.9			1.7			1.9				1.4	1.7		1.6								0.83		0.23			1				1.4					0.85	1.2						0.53
Tb	0.79	1.1			0.9			1				0.82	0.85		0.9								0.63		0.13			0.5				1.5					0.62	1.4						0.3
Yb	1.7	3.3			1.6			2				1.8	1.7		2								1.8		0.66			1.1				3.2					1.9	3.5						1.1
Lu	0.23	0.44			0.23			0.26				0.25	0.24		0.3								0.24		0.12			0.14				0.43					0.26	0.51						0.17

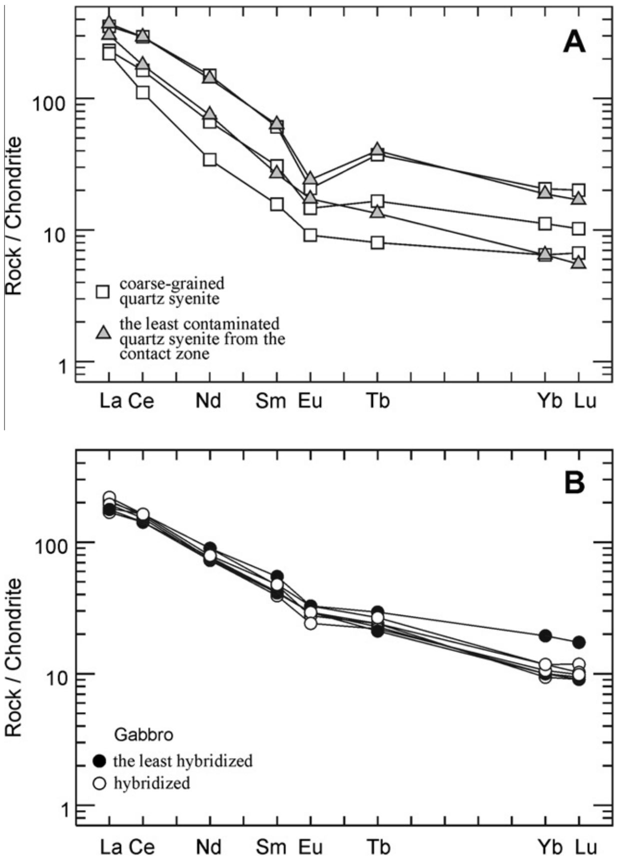

Fig. 7. REE patterns of magmatic rocks from the Shaluta pluton. (A) Quartz syenite. (B) Gabbro. Values for chondrite normalization are from Sun and McDonough (1989).

50 to 52 wt.%. MgO-based variation diagrams demonstrate significant dispersion in chemical composition of hybridized rocks. Nevertheless, rough positive correlation of MgO with CaO and negative correlation with K_2O, Na_2O, SiO_2, Al_2O_3, Ba, Sr, and Rb (not shown) are discernible. The trends are consistent with the modal mineral compositions of rocks and the chemical composition of rock-forming minerals. Increase in Na_2O, Al_2O_3 and Sr in hybridized gabbro is correlated with increase in the plagioclase ($An_{28–38}$) modal proportion, up to 77–80%. Likewise enrichment in K_2O and Ba correlates with increase in modal biotite and appearance of alkali feldspar. The significant content of biotite accounts for low SiO_2 (<55%) in gabbro despite its enrichment in alkalis. As a whole, compositional changes in gabbro manifest increase in the proportion of minerals making up the late mineral assemblage and enrichment in components typical of the host quartz syenite.

It is likely that varieties of gabbro that represent chemical composition of primary basalt melt can be distinguished by the enhanced contents of ‘refractory’ elements (Mg, Ca, Ni, Co, Cr). Of all available gabbro samples, only a few fulfill these requirements. Chemical compositions of four samples with the highest contents of the listed compatible elements are given in Table 3. The least hybridized gabbro samples are clearly distinguished by their compatible element contents (Fig. 8); however, their REE patterns overlap almost entirely with hybridized varieties attesting low mobility of REE during hybridization (Fig. 7B). Judging by the position in classification diagrams (Le Maitre, 1989; Rickwood, 1989), the composition of the primary mafic magma corresponds to high-K calc-alkaline basalt or even shoshonitic basalt.

6. Main results of melt inclusions study

A detailed description of the analytical procedures and a discussion of the data are given in a separate paper (Titov et al., 1998). Below only a concise summary and interpretation of the results that contribute to estimation of temperatures of mafic, silicic and hybrid magmas are given. A set of samples collected across the contact zone incorporates the following rock types: coarse-grained quartz syenite of the Shaluta pluton; medium-grained uncontaminated quartz syenite; quartz syenite veinlets and highly contaminated rock of quartz bearing monzonite composition from the immediate border zone; mafic rocks are represented by the hybridized gabbro.

Inclusions of crystallized melt, i.e. melt inclusions (MIs) have been studied mainly in quartz from all rock types, as well as in plagioclase and clinopyroxene from the hybridized gabbro sample. Narrow interval of homogenization temperature (T_h) in groups of inclusions within one grain and systematic decrease in T_h from the core to the margins of zoned crystals give grounds to consider that MI represent melt captured by a growing crystal and completely crystallized later on. For determination of the melt composition, the largest inclusions (6–10 μm) were homogenized, and then the glass was subjected to microprobe analysis. Unfortunately, partial loss of alkalis, mostly sodium, and fluids, is common during analysis. To obtain reliable data on T_h, groups of the smallest inclusions (up to 50–100 in quartz), 1–3 μm in diameter, were studied.

The main results of the microthermometric study and microprobe analyses of homogenized melt inclusions (artificial glass) are given in Tables 4 and 5. It was shown above that in all rock types quartz formed from a residual melt at a late stage of crystallization. For quartz from the medium-grained quartz syenite this conclusion is corroborated by the granitic composition of the homogenized MI (Table 5). Consequently, MI in quartz characterize near-solidus conditions. As evident from Table 4, T_h in MI from quartz in the coarse-grained quartz syenite is 700–720 °C. In rocks from the contact zone, T_h changes systematically as the extent of contamination increases. The lowest value of $T_h = 640–660$ °C is noted in quartz from the leucocratic medium-grained quartz syenite (samples B196-7 and B360-1). Homogenization temperature of MI in quartz from mildly contaminated rock is 670–700 °C; in the highly contaminated ones it increases to 780–800 °C (Table 4, samples A436, A and B, and sample B195-1). These data show that the near-solidus temperature of contaminated silicic magma systematically increased with increase in the mafic material proportion, which suggests that during interaction the mafic material was hot.

In the hybridized gabbro, homogenization temperatures in MI were studied in minerals from the late mineral assemblage. In andesine T_h of MI is 810–850 °C, in clinopyroxene it attains 850–900 °C, and in rare quartz grains T_h is the same as in highly contaminated silicic rocks, 760–790 °C. Judging from composition of melt inclusions in clinopyroxene, the late assemblage crystallized from the silica-enriched melt compared to gabbro (Table 5, #1 and 2). The composition is dacitic; however, taking into account significant loss of sodium during microprobe analysis, a quartz syenitic composition is more likely.

7. Discussion

7.1. Formation of medium-grained quartz syenite

The inner structure of the contact zones between the coarse-grained quartz syenite and gabbro in the Shaluta pluton (Figs. 2 and 3C) suggests that the origin of the medium-grained quartz

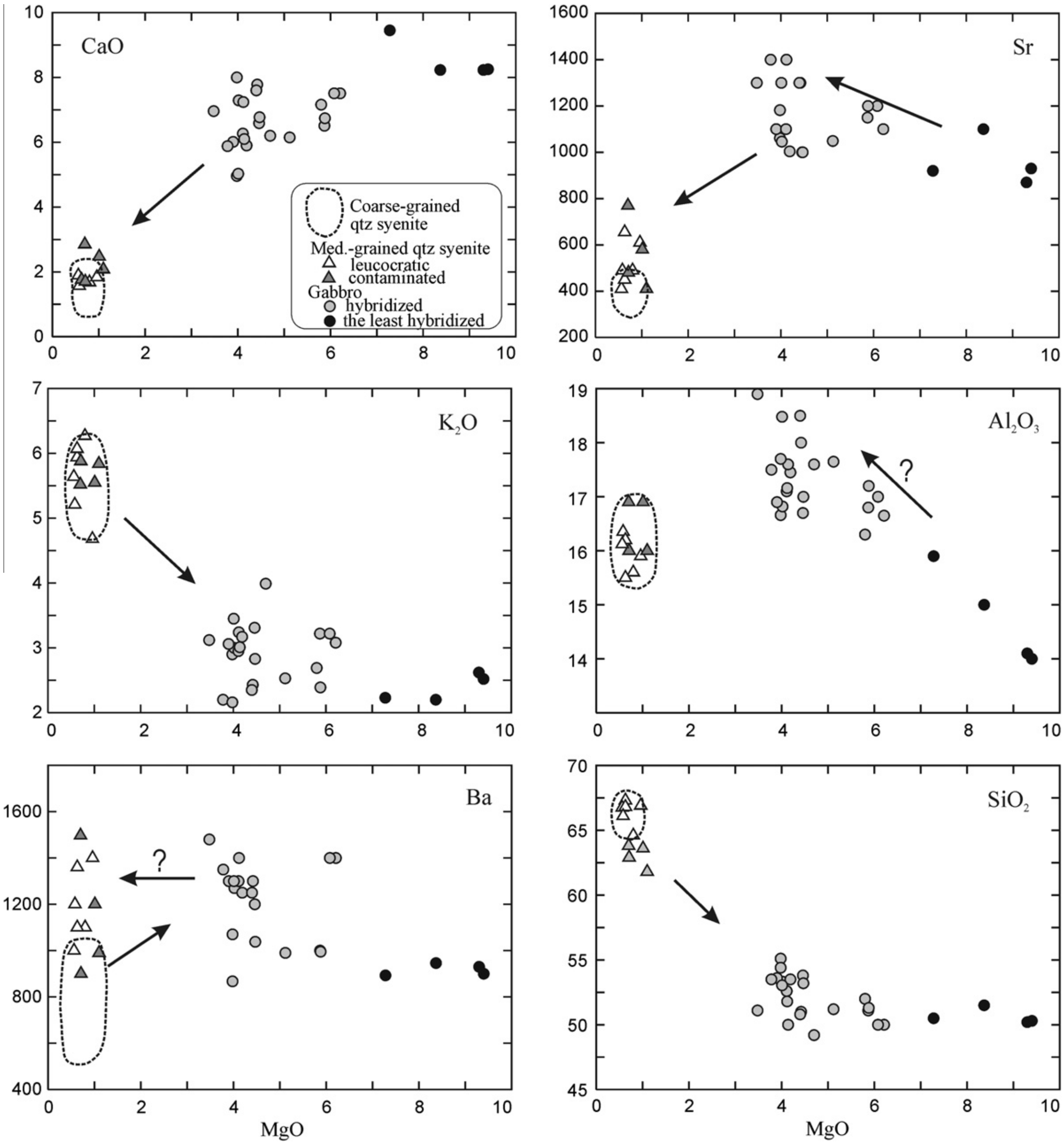

Fig. 8. Variation diagrams MgO vs. CaO, Sr, K_2O, Al_2O_3, Ba, SiO_2 for gabbro and medium-grained quartz syenite. Compositions of coarse-grained quartz syenite are shown as dash-line contours. Direction of the supposed diffusion of elements is shown by errows. Major oxides as wt.%, trace elements as ppm.

Table 4
Results of melt inclusions study in minerals (after Titov et al., 1998).

Sample #	Rock	Mineral	Melt inclusions	
			n	T_h (°C)
zz-1	Coarse-grained quartz syenite	Qtz	6	700–720
B196-7	Medium-grained quartz syenite from the contact zone	Qtz	5	640–660
B360-3		Qtz	7	640–660
A436-A	Quartz syenite veinlets in gabbro	Qtz	4	670–700
A436-B		Qtz	3	780–800
B195-1	Hybrid quartz bearing monzonite	Qtz	2	770–790 (a)
		Qtz	2	690–700 (b)
M60-15	Hybridized gabbro	Qtz	3	760–790
B266		Cpx	6	850–900
		An_{30-35}	3	810–850

n = Number of measurements; (c) and (m) = core and margin of the quartz grain.
T_h °C = homogenization temperature.

Table 5
Glass compositions in the homogenized melt inclusions (MI), wt.%.

Sample #	B266		B196-7			B360-3
	1	2	3	4	5	6
SiO_2	66.68	67.59	70.01	73.66	73.53	73.79
TiO_2	0.13	0.12	0.23	0.06	0.08	0.23
Al_2O_3	15.74	13.76	12.99	14.35	13.12	13.6
FeO^*	0.94	1.56	0.6	0.16	0.09	0.27
MnO	0.1	0.17	0.19	0.05	0.05	0.02
MgO	1.03	1.7	0.05	0.02	0.02	0.04
CaO	3.81	3.48	0.87	0.18	1.15	1.64
Na_2O	2.88	2.49	2.72	2.93	3.95	3.26
K_2O	3.9	3.74	5.42	3.85	3.23	2.9
Cl	0.04	0.08	0.4	0.14	0.2	0.21
Total	95.23	94.64	93.51	95.49	95.42	95.96

1 and 2 – MI 8 μm size in clinopyroxene from the hybridized gabbro; 3–6 – MI 8–10 μm size in quartz from the quartz syenite of the contact zone.

The homogenized melt inclusions (artificial glass) were analyzed on Camebax-micro-instrument at the Institute of Geochemistry, Novosibirsk.

The limit of detection 0.1–0.2 wt.%; significant loss of Na is likely. After Titov et al. (1998).

syenite is a critical issue for understanding the interaction between the host quartz syenite and intruded basalt magma. The typical magmatic texture of this rock and the presence of melt inclusions in the latest interstitial quartz grains is a clear evidence of their crystallization from magma rather than by metasomatic transformation of a solid rock in a contact zone.

Mafic microgranular enclaves are generally considered as evidence of co-mingling of fluid silicic melt with more viscous partially crystallized mafic magma (e.g., Wiebe, 1973; Furman and Spera, 1985; Frost and Mahood, 1987; Barbarin and Didier, 1991; Poli and Tommasini, 1991; Wiebe and Ulrich, 1997). In the Shaluta pluton abundant mafic enclaves in medium-grained quartz syenite exhibit evidence of ductile and plastic deformation and commonly have crenulate, cuspate, lobate and sinuous contours that are characteristic of contact surface of two viscous liquids (Figs. 2 and 3). Also, decrease of grain size in the margins of gabbro intrusives and in the outer zone of larger mafic enclaves (quench rims) suggests faster crystallization of basic melt immediately near the contact with 'colder' host silicic magma. These observations suggest that silicic magma in the contact zone co-existed with mafic magma that formed the gabbro intrusives. Study of melt inclusions in the quartz grains provides direct evidence of the high temperature of the gabbro during the formation of the medium-grained syenite (Table 4). The homogenization temperature of melt inclusions systematically increases from 640 to 660 °C in the least contaminated quartz syenite to 780–800 °C in highly contaminated rocks with significant amount of gabbro material. Taking into account that quartz in these rocks is a near-solidus mineral, it is concluded that the temperature of magma was considerably higher.

Field evidence indicates that the coarse-grained quartz syenite making up the Shaluta pluton was not completely crystallized when the mafic magma intruded. This follows from the presence of very thin synplutonic microgabbro dykes in the coarse-grained quartz syenite. Numerous injections of the host silicic melt into these dykes attest that mafic dykes intruded into partially melted quartz syenite (Marshall and Sparks, 1984; Furman and Spera, 1985; Frost and Mahood, 1987; Barbarin and Didier, 1991). The presence of synplutonic mafic dykes, as well as typical dyke-like apophyses of mingled magma that intruded into the quartz syenite pluton from the contact zone (Fig. 2), demonstrate that, despite the presence of residual melt, the host quartz syenite behaved rheologically as solid, with less than 30% residual melt (Van der Molen and Peterson, 1979; Fernandez and Gasquet, 1994).

The silicic melt that formed the medium-grained quartz syenite was produced by remelting of incompletely crystallized coarse-grained quartz syenite near the contact with the intruded synplutonic gabbro.

The similarity in chemical and mineral compositions between the coarse-grained and the least contaminated medium-grained quartz syenites (Table 3; Figs. 6, 7a, and 4) suggests high extent of remelting immediately near the contact with gabbro.

7.2. Thermal regime of remelting

Amphibole geobarometry (Hollister et al., 1987; Hammarstrom and Zen, 1986) in the coarse-grained syenite gives a pressure estimation of 2.2–2.3 kbar. These values suggest crystallization at depth of about 7–10 km.

Petrological considerations constrain the temperature of the mafic magma. The proportion of phenocrysts in the porphyritic microgabbro immediately near the contact with the host quartz syenite is ~10 vol.%; this testifies the near-liquidus temperature of the intruded mafic magma. Plagioclase is the only phenocryst suggesting that the water content of the magma was relatively low, ⩽3 wt.% (Eggler, 1972; Stern et al., 1975). The liquidus temperature of basalt melt with 2–3 wt.% H_2O is about 1100–1200 °C at P = 2–3 kbar (Ringwood, 1975; Stern et al., 1975).

The temperature of the nearly solidified coarse-grained quartz syenite, in which small amount (⩽30%) of residual melt remained, should be close to solidus temperatures and can be estimated by the T_h of melt inclusions in the near-solidus quartz grains, 700–720 °C (Table 4).

To assess the temperature of the contact remelting, we performed thermal conduction calculations following Furman and Spera (1985):

$$T = T_2 + (T_1 - T_2)/2\{erfa - x/2\sqrt{k} * t + erfa + x/2\sqrt{k} * t\},$$

in which T is temperature of refusion at a distance $x - a$; a = basalt sill half-width ($2a$ is taken as 100 m); x = distance from center of basalt sill; $x - a$ = observed width of the refusion zone, from 1 to 3 m; T_1 = temperature of basalt magma, 1200 °C; T_2 = temperature of host quartz syenite, 700 °C, at $t = 0$; k^* = effective thermal diffusivity, $5 \times 10^{-7}\,m^2\,s^{-1}$; t = time of the basalt sill crystallization that is calculated according to Irvin (1970) as $t = 2aL\sqrt{k}/4C\,(T_1 - T_2)$.

The calculations show that when $x - a \sim 3$ m, the maximum observed width of the refusion zone, $T \approx 950$ °C. The estimation of the remelting temperature seems realistic. It is comparable with the homogenization temperature of melt inclusions from the later pyroxene, 850–900 °C (Table 4), characterizing the onset of hybridization process superimposed on the incompletely crystallized gabbro near the contact with quartz syenite. Thus the maximum refusion temperature is estimated at 900–950 °C.

Data on melt and fluid inclusions suggest that the magmatic stage of the interaction process lasted to fairly low temperature and was likely influenced by fluid. In particular, the low value of T_h = 640–660 °C of melt inclusions in quartz from the least contaminated medium-grained syenite that is 50–60 °C less than in quartz from the coarse-grained quartz syenite (Table 4), gives ground to assume that the refusion was accompanied by influx of H_2O. This assumption is supported by the abundance of syngenetic water-rich fluid inclusions in quartz syenite from the contact zone (Titov et al., 1998). Influx of H_2O decreased both solidus and liquidus temperatures of the newly formed melt and was favorable for the high extent of refusion.

7.3. Chemical interaction between mafic and silicic magmas

Chemical admixing is widely manifested in the contact zone; however, it affected the medium-grained quartz syenite and the gabbro in different ways. The estimated temperature of the contact melting, ~900–950 °C, is comparable with near-solidus temperature of basalt magma with moderate water content at P = 2–3 kbar (Stern et al., 1975; Sisson and Grove, 1993) and suggests that the newly formed quartz syenite melt was liquid during almost the entire period of gabbro crystallization. This caused extensive interaction between the two magmas (the remelted quartz syenite and gabbroic crystal "mush") and between the crystal phase and hybridized residual melt in gabbro. However, rapid cooling stopped the mixing process far from equilibrium, at the stage when the borders between felsic and mafic end members were still well distinguished (Fig. 2).

Comparison of chemical and mineral compositions of the least contaminated quartz syenite from the contact zone and the coarse-grained syenite making up the bulk of the pluton shows that the former was enriched in Sr and Ba at the early stage of chemical interaction (Table 3, Fig. 6B). Judging by the compositions of plagioclase and mafic minerals (Figs. 4 and 5), Ca and Ti gain also occurred, although it is recognized by whole-rock chemical data only in contaminated medium-grained quartz syenite (Fig. 6). It is likely that in addition to Sr, Ba, Ca and Ti the crystallized basalt magma was also the source of water that enriched the refusion zone (see forgoing section). If the initial water content in the basalt magma was ~2–3 wt.%, then water saturation at a pressure of 2–3 kbar should have been attained at a crystallization extent of 50–60% (Stern et al., 1975; Holloway and Blank, 1994 and Ref. therein). Water-rich fluid released from the crystallized basalt melt could readily migrate within the silicic magma and dissolve in it. The mafic magma was also the main source of Cl: biotite from the refusion zone is very similar in Cl content to biotite from gabbro rather than that from coarse-grained quartz syenite (Fig. 5). The source of fluorine, however, was the quartz syenite pluton. Since the refusion zone was fairly thin, commonly less than three meter wide, diffusion was the most likely process of elements and fluids transport (Watson, 1982; Watson and Jurewicz, 1984; Van der Laan and Wyllie, 1993). The contaminated medium-grained quartz syenite is characterized by enhanced content of typical gabbro components (Table 3; Figs. 4 and 5). The abundance of mafic enclaves and small relicts of gabbroic material in this rock type thus suggests that Ca, Mg and Ti increase occurred both by the local mingling–mixing processes and by diffusion from the adjacent gabbro intrusion.

Turning to the gabbro, it should be remembered that crystal "mush" rather than the liquid mafic magma interacted with the newly formed silicic magma (Figs. 2 and 3C). Two types of interaction, melt–melt and hybrid melt – crystals, can be recognized. At first the residual melt in mafic "mush" was subjected to hybridization, mostly via interdiffusion with the quartz syenite magma. Then the hybrid melt reacted with the crystal phase, which resulted in the formation of a late mineral assemblage (andesine, edenite, late pyroxene, biotite, minor alkali feldspar and quartz).

Chemical interaction within the contact zone of gabbro included diffusion of components from the silicic melt (Ba, K) and from the inner parts of the gabbro itself (Al, Sr), both fixed in the crystals of the late mineral assemblage. Crystallization provided removal of the diffused components from the melt and, as a result, maintenance of the gradient of concentrations that defined further diffusion (Eberz and Nicholls, 1990; Zorpi et al., 1991). The diffusion persisted up to the latest stages of crystallization and brought to the anomalous accumulation of Sr, Ba and Al in the border zone of gabbro (Fig. 8). In mineralogical respect, accumulation of Sr and Al is manifested in higher proportion of andesine, up to 80 vol.% (as compared with 50–60% labradorite in the initial gabbro), whereas enrichment in Ba and K was caused by crystallization of biotite and minor alkali feldspar. The supposed directions of element diffusion are shown by arrows in Fig. 8, although some of the arrows are debatable. In particular, it remains unclear whether the significant Ba increase in the medium-grained quartz syenite was caused by diffusion from the adjacent hybridized gabbro; lack of correlation between Ba and K_2O (Fig. 6B) argues for direct element diffusion or transfer by fluids. As for the increase of alumina content in the hybridized gabbro, it can be interpreted either as a result of diffusion from the inner zones or the effect of redistribution of major oxides in the course of crystal-melt interaction. In any event, the bell-shaped distribution of Sr and Al_2O_3 in the plots (Fig. 8) is more likely explained by reactions between solid phase and hybrid melt rather than by endo-hybridization, i.e. simultaneous mixing and fractionation (Duchesne et al., 1998). The process of two magmas interaction in the Shaluta pluton had been "freezed" still at the mingling stage.

As a whole, the obtained results support the models suggested earlier (Eberz and Nicholls, 1990; Holden et al., 1991; Zorpi et al., 1991; Litvinovsky et al., 1995). According to these models, mingling of mafic and silicic magmas, unlike magma mixing, is accompanied by chemical interaction of silicic magma with the residual melt in the crystallized basalt magma. As a result, the residual melt composition is progressively changed mainly owing to the interdiffusion reactions. Our data testify that, in addition to chemical interaction of two melts, reactions between liquid and crystal phases also played a great role.

8. Conclusion

In the Shaluta pluton, evidence for remelting of coarse-grained quartz syenite at the contact with gabbro intrusion was found. The quartz syenite pluton was still hot and contained ⩽30% of the residual melt when intruded by gabbro. The refusion was followed by mingling and chemical interaction of mafic and newly formed silicic magmas within the narrow contact zone. The mingled magmatic material was partly squeezed out from the contact zone inwards, into the incompletely crystallized quartz syenite pluton, forming dyke-like apophyses of several tens of meters long; they look like typical composite dykes. This mechanism can be considered as a possible natural model for the formation of composite dykes with silicic margins.

Acknowledgments

The authors are deeply grateful to V. Popov and F. Reyf for fruitful discussions. Thoughtful reviews and valuable recommendations of Y. Be'eri-Shlevin, J.P. Liégeois and G.E. Poli greatly improved the manuscript.

References

Barbarin, B., Didier, S., 1991. Review of the main hypothesis proposed for the genesis and evolution of mafic microgranular enclaves. In: Didier, S., Barbarin, B (Eds.), Enclaves and Granite Petrology. Development in Petrology, vol. 13. Elsevier, Amsterdam, pp. 367–373.

Blake, D.H., Elwell, R.W.D., Gipson, I.L., Skelhorn, R.R., Walker, G.P.L., 1965. Some relationships resulting from the intimate association of acid and basic magmas. Quarterly Journal of Geological Society of London 121, 31–49.

Duchesne, J.-C., Berza, T., Liégeois, J.-P., Auwera, J.V., 1998. Shoshonitic liquid line of descent from diorite to granite: the late Precambrian post-collisional Tismana pluton South Carpathians, Romania. Lithosphere 45, 281–303.

Eberz, G.W., Nicholls, I.A., 1990. Chemical modification of enclave magma by post-emplacement crystal fractionation, diffusion and metasomatism. Contributions to Mineralogy and Petrology 104, 47–55.

Eggler, D.H., 1972. Water-saturated and undersaturated melting reaction in a Paricutin andesite and an estimate of water content in the natural basalt magma. Contributions to Mineralogy and Petrology 34, 261–271.

Fernandez, A.N., Gasquet, D.R., 1994. Relative rheological evolution of chemically contrasted coeval magmas: example of the Tichka plutonic complex (Morocco). Contributions to Mineralogy and Petrology 116, 316–326.

Frost, T.P., Mahood, G.A., 1987. Styles of mafic–felsic magma interaction: the Lamarck granodiorite, Sierra Nevada, California. Geological Society of America Bulletin 99, 272–291.

Furman, T., Spera, F.J., 1985. Co-mingling of acid and basic magma with the implications for the origin of mafic I-type xenoliths: field and petrochemical relations of an unusual dyke complex at Eagle Lake, Sequoia National Park, California, USA. Journal of Volcanology and Geothermal Research 24, 151–178.

Hammarstrom, J.M., Zen, E., 1986. Aluminum in hornblende: an empirical igneous geobarometer. American Mineralogist 71, 1297–1313.

Holden, P., Halliday, A.N., Stephens, W.E., Henney, P.J., 1991. Chemical and isotopic evidence for major mass transfer between mafic enclaves and felsic magma. Chemical Geology 92 (1/3), 135–152.

Hollister, L.S., Grissom, G.C., Peters, E.K., Stowell, H.H., Sisson, V.B., 1987. Confirmation of the empirical correlation of Al in hornblende with pressure of solidification of calc-alkaline plutons. American Mineralogist 72, 231–239.

Holloway, J.R., Blank, J.G., 1994. Application of experimental results to C–O–H species in natural melts. The Mineralogical Society of America Reviews in Mineralogy 30 (6), 187–230.

Huppert, H.E., Sparks, R.S.J., 1988. The generation of granitic magmas by intrusion of basalt into continental crust. Journal of Petrology 29, 596–624.

Kanaris-Sotiriou, R., Gill, F.G.F., 1985. Hybridization and the petrogenesis of composite intrusions: the dyke at *An* Cumhann Isle of Arran, Scotland. Geological Magazine 122, 361–372.

Katzir, Y., Litvinovsky, B.A., Jahn, B.M., Eyal, M., Zanvilevich, A.N., Valley, J.W., Vapnik, Ye., Beerik, Y., Spicuzza, M.J., 2007. Interrelations between coeval mafic and A-type silicic magmas from composite dykes in a bimodal suite of southern Israel, northernmost Arabian–Nubian Shield: geochemical and isotope constrains. Lithos 97, 336–364.

Kouchi, A., Sanagawa, I., 1983. Mixing basaltic and dacitic magmas by forced convection. Nature 304, 527–528.

Koyaguchi, T., Takada, A., 1994. An experimental study of the formation of composite intrusions from zoned magma chambers. Journal of Volcanology and Geothermal Research 59, 261–267.

Le Maitre, R.W. (Ed.), 1989. A Classification of Igneous Rocks and Glossary of Terms Blackwell, Oxford.

Litvinovsky, B.A., Zanvilevich, A.N., Kalmanovich, M.A., 1995. Recurrent mixing and mingling of coexisting syenite and basalt magmas in the Ust'-Khilok massif, Transbaikalia, and its petrologic significance. Petrology 3, 115–137.

Litvinovsky, B.A., Zanvilevich, A.N., Wickham, S.M., Steele, I.M., 1999a. Genesis of the syenitic magmas of anorogenic granitoid series: syenite-granitic series of Transbaikalia. Petrology 7, 459–481.

Litvinovsky, B.A., Posokhov, V.F., Zanvilevich, A.N., 1999b. New Rb–Sr data on the age of Late Paleozoic granitoids in Western Transbaikalia. Russian Geology and Geophysics 40, 677–685.

Litvinovsky, B.A., Tsygankov, A.A., Jahn, B.M., Katzir, Y., Be'eri-Shlevin, Y., 2011. Origin and evolution of overlapping calc-alkaline and alkaline magmas: the Late Palaeozoic post-collisional igneous province of Transbaikalia (Russia). Lithos 125, 845–874.

Marshall, L.A., Sparks, R.S.J., 1984. Origin of some mixed-magma and net-veined ring intrusions. Journal of Geological Society of London 141, 171–182.

Petrelli, M., Perugini, D., Poli, G., 2011. Transition to chaos and implications for time-scales of magma hybridization during mixing process in magma chambers. Lithosphere 125, 211–220.

Poli, G.E., Tommasini, S., 1991. Model of the origin and significance of microgranular enclaves in calc-alkaline granitoids. Journal of Petrology 32 (3), 657–666.

Rickwood, P.C., 1989. Boundary lines within petrologic diagrams which use oxides of major and minor elements. Lithos 22, 247–263.

Ringwood, A.E., 1975. Composition and Petrology of the Earth's Mantle. Mc Graw-Hill Book Company, NY, 580 pp.

Sisson, T.W., Grove, T.L., 1993. Experimental investigations of the role of H_2O in calc-alkaline differentiation and subduction zone magmatism. Contributions to Mineralogy and Petrology 113, 143–166.

Snyder, D., Tait, S., 1995. Replenishment of magma chambers: comparison of fluid-mechanic experiments with field relations. Contribution to Mineralogy and Petrology 122, 230–240.

Snyder, D., Crambles, C., Tait, S., Wiebe, R.A., 1997. Magma mingling in dikes and sills. Journal of Geology 105, 75–86.

Stern, Ch., Huang, W.-L., Wyllie, P., 1975. Basalt–andesite–rhyolite–H_2O: crystallization intervals with excess H_2O and H_2O-undersaturated liquidus surfaces to 35 kbars, with implications for magma genesis. Earth and Planetary Science Letters 28, 189–196.

Sun, S., McDonough, W.F., 1989. Chemical and isotopic systematics of oceanic basalts: implications for mantle compositions and processes. In: Saunders, A.D., Norry, M.J. (Eds.), Magmatism in the Ocean Basins. Geological Society of London, Special Publication 42, pp. 313–45.

Titov, A.V., Litvinovsky, B.A., Zanvilevich, A.N., 1998. PT-conditions and mechanisms of interaction of contrasting magmas in the Shaluta pluton, Transbaikalia (from the results of study of melt inclusions in minerals). Russian Geology and Geophysics 39 (3), 361–370.

Titov, A.V., Litvinovsky, B.A., Zanvilevich, A.N., Shadaev, M.G., 2000. Hybridization in composite basic-leucogranite dykes in the Ust-Khilok pluton (Transbaikalia). Russian Geology and Geophysics 41 (12), 1714–1728.

Van der Laan, S.R., Wyllie, P.J., 1993. Experimental interaction of granite and basaltic magmas and implications for mafic enclaves. Journal of Petrology 34 (3), 491-17.

Van der Molen, I., Peterson, M.S., 1979. Experimental deformation of partially-melt granite. Contribution to Mineralogy and Petrology 70, 299–318.

Vogel, T.A., Wilband, J.T., 1978. Coexisting acidic and basic melts: geochemistry of a composite dyke. Journal of Geology 86, 353–371.

Wager, L.R., Brown, G.M., Bell, J.D., 1965. Marscoite and related rocks of the Western Red Hills complex, Isle of Skye. Philosophical Transactions of the Royal Society of London A257, 273–307.

Watson, E.B., 1982. Basalt contamination by continental crust: some experiments and models. Contributions to Mineralogy and Petrology 80, 73–77.

Watson, E.W., Jurewicz, S.R., 1984. Behavior of alkalis during diffusive interaction of granitic xenolith with basaltic magma. Journal of Geology 92, 121–131.

Wickham, S.M., Litvinovsky, B.A., Zanvilevich, A.N., Bindeman, I.N., 1995. Geochemical evolution of Phanerozoic magmatism in Transbaikalia, East Asia: a key constraint on the origin of K-rich silicic magmas and the process of cratonization. Journal of Geophysical Research 100 (B8), 15,641–15,654.

Wiebe, R.A., 1973. Relations between coexisting basaltic and granitic magmas in a composite dyke. American Journal of Science 273, 130–151.

Wiebe, R.A., 1993. The Pleasant Bay layered gabbro-diorite coastal Maine: ponding and crystallization of basalt injections into a silicic magma chamber. Journal of Petrology 34, 461–489.

Wiebe, R.A., Ulrich, R., 1997. Origin of composite dykes in the Gouldsboro granite, coastal Maine. Lithosphere 40, 157–178.

Zorpi, M.J., Couloh, C., Orsini, J.B., 1991. Hybridization between felsic and mafic magmas in calc-alkaline granitoids – a case study in northern Sardinia, Italy. Chemical Geology 92 (1/3), 45–86.